Tissue Eng Regen Med (2023) 20(4):523–538
https://doi.org/10.1007/s13770-023-00522-3

Online ISSN 2212-5469

REVIEW ARTICLE

Tissue-Engineered 3D *In Vitro* Disease Models for High-Throughput Drug Screening

Gillian Huskin[1] · Jun Chen[1] · Trenton Davis[1] · Ho-Wook Jun[1]

Received: 2 December 2022 / Revised: 5 January 2023 / Accepted: 16 January 2023 / Published online: 9 March 2023
© Korean Tissue Engineering and Regenerative Medicine Society 2023

Abstract During high-throughput drug screening, *in vitro* models are fabricated and the effects of therapeutics on the models evaluated in high throughput—for example, with automated liquid handling systems and microplate reader-based high-throughput screening (HTS) assays. The most frequently-used model systems for HTS, 2D models, do not adequately model the *in vivo* 3D microenvironment—an important aspect of which is the extracellular matrix—and therefore, 2D models may not be appropriate for drug screening. Instead, tissue-engineered 3D models with extracellular matrix-mimicking components are destined to become the preferred *in vitro* systems for HTS. However, for 3D models, such as 3D cell-laden hydrogels and scaffolds, cell sheets, and spheroids as well as 3D microfluidic and organ-on-a-chip systems, to replace 2D models in HTS, they must be compatible with high-throughput fabrication schemes and evaluation methods. In this review, we summarize HTS in 2D models and discuss recent studies that have successfully demonstrated HTS-compatible 3D models of high-impact diseases, such as cancers or cardiovascular diseases.

Keywords High-throughput screening assays · 3D cell culture · Hydrogels · Cancer · Cardiovascular diseases

1 Introduction

Drug research and development (R&D) is incredibly expensive—the U.S. Congressional Budget Office has estimated that the annual cost of drug R&D in 2019 was over eighty billion USD [1]. There are several reasons this amount is as high as it is—one of which is that, for many drugs, safety and efficacy as demonstrated *in vitro* is not substantiated by *in vivo* animal and clinical trials [2–4]. This has been attributed, in part, to the use of two-dimensional (2D) models, such as cells adhered to tissue culture plastics, for *in vitro* high-throughput drug screening. Specifically, the use of 2D *in vitro* models for high-throughput screening (HTS) has been criticized because 2D models do not adequately model the *in vivo* three-dimensional (3D) microenvironment, especially the extracellular matrix (ECM). The ECM is partially composed of ECM proteins, such as collagen, laminin, fibrin, and fibronectin, which may therefore be considered ECM-mimicking components [5, 6]. In addition, the partially hydrolyzed version of collagen, gelatin, has been used as an ECM-mimicking component as have alginate, methacrylate, and synthetic biomaterials, such as peptide amphiphiles (PAs) with the Tyr-Ile-Gly-Ser-Arg (YIGSR) cell-adhesive sequence associated with laminin [6–9]. 3D *in vitro* models with ECM-mimicking components may be more appropriate for drug screening, and indeed, when 3D *in vitro* models with ECM-mimicking components have been used in several HTS studies, drug safety and efficacy has contrasted with that concluded from studies of 2D *in vitro* models [7, 10]. Therefore, advanced, tissue-engineered 3D *in vitro* models, such as 3D cell-laden hydrogels and scaffolds, in which cells are fully encapsulated in or surrounded by ECM-mimicking materials, are destined to become the preferred *in vitro* models for HTS [6].

✉ Ho-Wook Jun
hwjun@uab.edu

[1] Department of Biomedical Engineering, The University of Alabama at Birmingham, Birmingham, AL 35294, USA

However, there are significant obstacles that may prevent the use of 3D models for HTS, such as the high-throughput fabrication of HTS-compatible 3D models and the high-throughput evaluation of these models with HTS assays [4].

In this review, we first summarize HTS in 2D models. Then, we explore the problems that have arisen from the use of 2D models for this application as well as the multiple ways in which 3D models may provide a solution, especially for HTS of therapeutics for high-impact diseases, such as cancers and cardiovascular diseases (CVDs). Next, we introduce the types of 3D *in vitro* models for HTS and discuss recent studies that have successfully used these 3D models in high-throughput drug screening applications. Finally, we conclude with an overview of the 3D HTS assays from these studies to facilitate the development of additional HTS-compatible 3D disease models for high-throughput drug screening. In addition, this review is intended to highlight the value of advanced, tissue-engineered, HTS-compatible 3D *in vitro* models, such as the models we are currently developing for atherosclerosis and other CVDs.

2 High-throughput drug screening with 2D *in vitro* models

2D *in vitro* models, ranging from cells cultured on tissue culture plastics—the most fundamental of 2D models—to more advanced models, such as 2D cell sheets, have long served as stand-ins for a variety of animal and human tissues [11]. High-throughput drug screening, in particular, has made extensive use of 2D models; the most frequently used model systems in HTS are 2D models—specifically, cells cultured in 96-, 384-, or 1536-well microtiter plates [4, 12, 13]. While the use of these 2D *in vitro* models for drug screening has been called into question, [2–4] there are several characteristics that make this type of 2D *in vitro* model attractive for HTS. For example, with 2D *in vitro* models, many compounds may be screened in each microtiter plate and evaluated with microplate readers and HTS assays related to absorbance, fluorescence, or luminescence [13]. The number of drugs screened with an *in vitro* model is important because high-throughput drug screening has a minimum daily throughput of 10,000 drugs. This number is somewhat variable, and some definitions have even placed the threshold for minimum daily throughput in HTS as high as 100,000 drugs [12, 14]. Minimum daily throughput requirements may be difficult or impossible to meet without some degree of automation, so many of the steps in HTS may be machine automated—for example with automated liquid handling systems (Fig. 1A) [12, 13]. In addition, many HTS assays have been designed to make the results of high-throughput drug screening readily apparent even when automated systems are used—for example, by way of fluorescence, which may be detected in a fully-automated and high-throughput fashion with a microplate reader.

Fig. 1 2D HTS and Cell-Based HTS Assays. **A** An example scheme for 2D HTS, in which automated liquid handling systems produce 2D *in vitro* models in 96- or 384- well microtiter plates, which can then be incubated. [7, 13]. Drugs and HTS assay reagents can be applied similarly, after which measurement systems for *in vitro* models in microtiter plates, such as microplate readers, can be employed. **B** An overview of selected 2D cell-based HTS assays, including an example of a cell-based assay from a 2D HTS atherosclerosis study, in which the fluorescent dye DiI was used as the basis of a HTS assay for oxidized low-density lipoprotein (oxLDL) uptake [21] ▶

2D HTS assays are either (1) target-based HTS assays or (2) cell-based HTS assays [15]. In target-based HTS assays, such as fluorescence resonance energy transfer and fluorescence polarization assays, one compound is designated as the target, and other compounds are assayed to determine if they can successfully bind the target [15, 16]. This type of HTS assay does not require a cell-based 2D *in vitro* model, only the target compound. Because the cell-based 2D *in vitro* model is typically substituted for the target compound in a target-based HTS assay, we will focus on cell-based HTS assays in this review. Cell-based HTS assays are used to evaluate the effects of compounds on important aspects of 2D *in vitro* models, such as cell viability and proliferation. Cell viability and proliferation, specifically, may be assayed in high throughput with a variety of fluorescent or colorimetric assays—the results of which may be evaluated with a microplate reader [17]. A representative example of a colorimetric cell-based HTS assay is the 3-(4,5-dimethylthiazol- 2-yl)-2,5- diphenyl-2H-tetrazolium (MTT) assay, which is based on the ability of living cells to produce the blue or purple compound, formazan, from an MTT salt by reduction (Fig. 1B) [17, 18]. Apart from similar colorimetric HTS assays for metabolism, such as the Resazurin or alamarBlue assay, several other methods have been used to evaluate cell viability and proliferation in 2D *in vitro* models [17, 19]. A representative example of a luminescent assay is the CellTiterGlo® assay, an adenosine triphosphate (ATP) assay [2, 17]. In an ATP assay, fluorescence is detected when the non-luminescent compound, luciferin, is converted into the luminescent compound, oxyluciferin, in a reaction that requires ATP and therefore may be used for ATP quantification. There are also high-throughput live/dead assays based on fluorescent stains, such as calcein AM, propidium iodide (PI), or ethidium homodimer-1 (EthD-1) [2, 20]. Finally, there are cell proliferation assays, such as CyQUANT and PicoGreen assays, in which

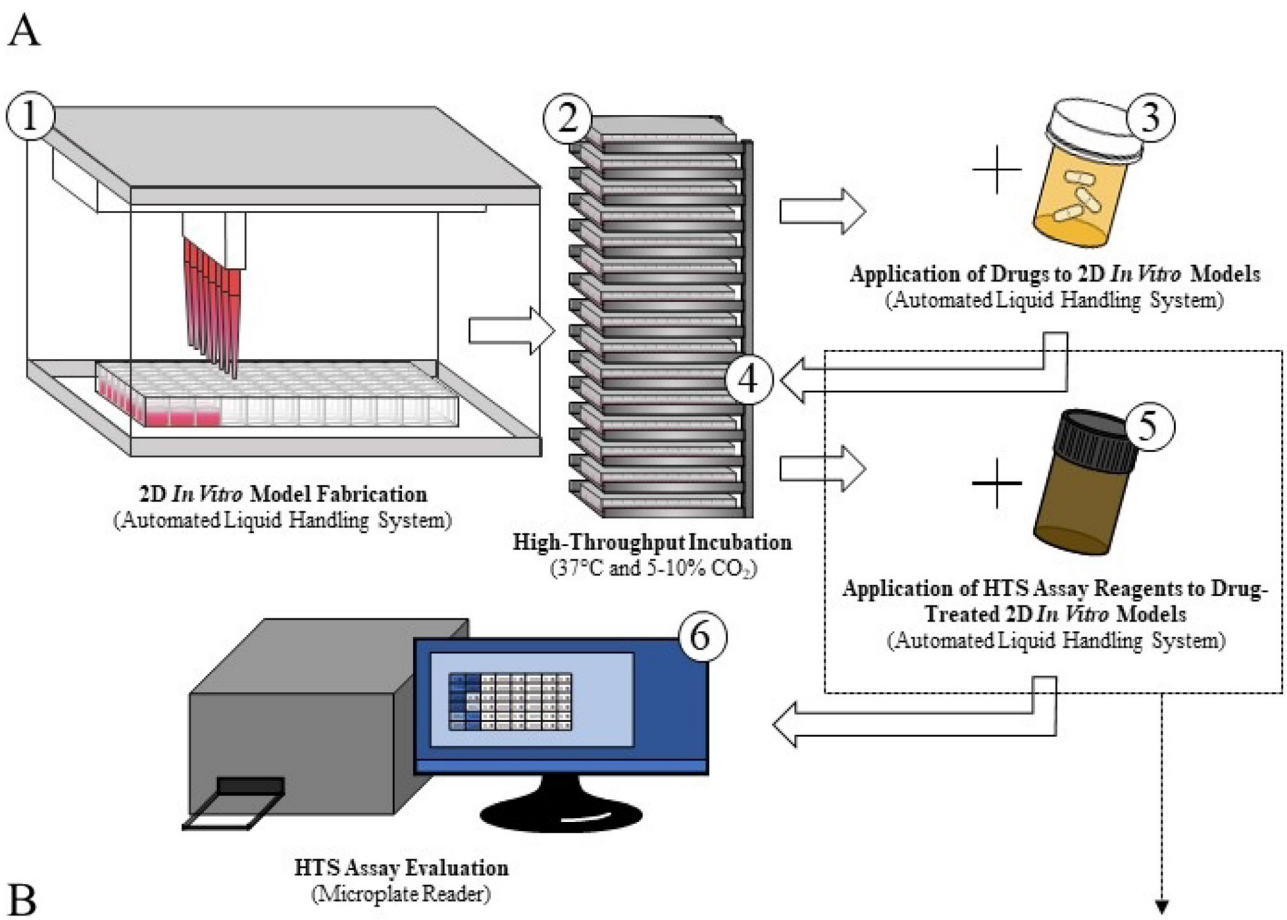
A
1
2
3
4
5
6
2D *In Vitro* Model Fabrication
(Automated Liquid Handling System)
High-Throughput Incubation
(37°C and 5-10% CO_2)
Application of Drugs to 2D *In Vitro* Models
(Automated Liquid Handling System)
Application of HTS Assay Reagents to Drug-Treated 2D *In Vitro* Models
(Automated Liquid Handling System)
HTS Assay Evaluation
(Microplate Reader)

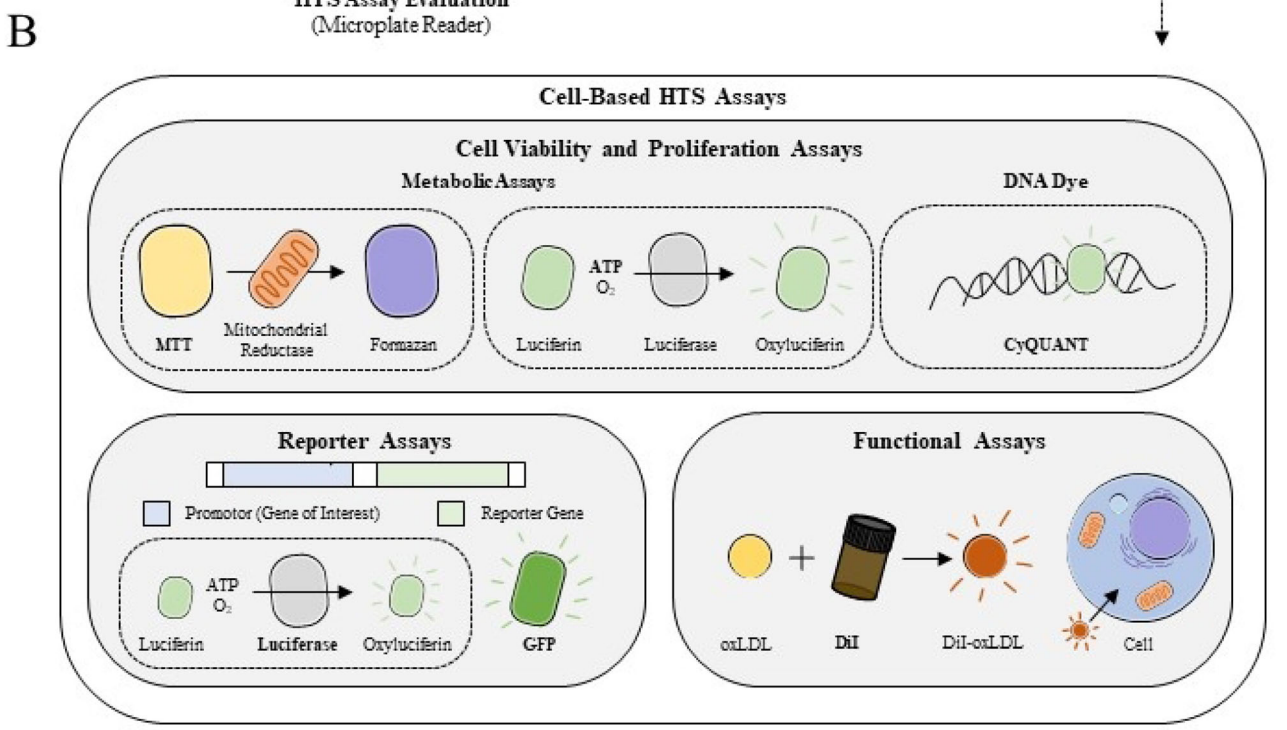
B
Cell-Based HTS Assays
Cell Viability and Proliferation Assays
Metabolic Assays
DNA Dye
MTT
Mitochondrial Reductase
Formazan
ATP
O_2
Luciferin
Luciferase
Oxyluciferin
CyQUANT
Reporter Assays
Promotor (Gene of Interest)
Reporter Gene
ATP
O_2
Luciferin
Luciferase
Oxyluciferin
GFP
Functional Assays
oxLDL
DiI
DiI-oxLDL
Cell

proliferation, or more specifically, the amount of DNA in the *in vitro* models, is calculated based on the conditional fluorescence of the CyQUANT and PicoGreen HTS assay reagents when bound to DNA [22–24].

In addition to high-throughput cell viability and proliferation assays, there are several other cell-based HTS assays—the most prominent of which are reporter assays [25]. In reporter assays, 2D *in vitro* models are genetically modified to express a reporter gene, such as green fluorescent protein (GFP), with the promotor for a gene of interest [25–27]. The proteins translated from reporter genes have one or more characteristics, such as fluorescence or enzymatic activity, with which the expression of the reporter gene can be determined in a high-throughput manner. Because the expression of the reporter gene is indicative of the expression of the gene of interest, the expression of the gene of interest can, thus, be determined in high-throughput. Reporter assays include GFP-based reporter assays, in which fluorescence of the 2D model may be directly assessed with a microplate reader, as well as luciferase-based reporter assays, in which luciferin must first be applied to the 2D model and converted to a luminescent compound, oxyluciferin, by luciferase [25, 28]. Secreted luciferase and secreted alkaline phosphatase (SEAP) reporter assays, which allow the cell culture supernatant to be evaluated instead of the cells from a 2D *in vitro* model, are also worthy of mention [25]. The remainder of the cell-based HTS assays discussed in this review evaluate functions of *in vitro* models and the effects of therapeutics on these functions, such as the ability of models to uptake synthetic or biological compounds like nanoparticles (NPs) or oxidized low-density lipoprotein (oxLDL) [21, 29].

3 High-throughput drug screening with 3D *in vitro* models

3.1 The suitability of 3D in vitro models for high-throughput drug screening

Even though the most frequently-used model in high-throughput drug screening is a 2D *in vitro* model, 3D *in vitro* models may be better for this application because 2D models do not adequately model the *in vivo* 3D microenvironment, especially the ECM [2–4, 12]. Correspondingly, HTS studies have demonstrated that the safety and efficacy of drugs as determined with high-throughput drug screening varies, often in a statistically significant manner, depending on the dimensionality of *in vitro* model used [7, 10]. Although many of the mechanisms involved in these differences have not been fully elucidated, the 3D microenvironment of a cell, which consists of the ECM of the cell and that of other cells as well as interstitial fluid and the biochemical components thereof, has been reported as one of the determinants of cellular behavior—for example, through mechanotransduction [5, 30]. It should be noted that the 3D microenvironments in many pathophysiologies, such as cancers and CVDs, may be even more important to model accurately because, not only are they dissimilar to the 3D microenvironment in a non-disease state, but they are often involved in disease progression [31, 32]. Differences between the 3D microenvironments in disease states and non-disease states are, perhaps, most readily apparent in the 3D cancer microenvironment, the tumor microenvironment (TME) [33].

Cells in the TME are subject to a range of biomechanical forces, such as compression, as the tumor increases in size—biomechanical forces not experienced by cells in non-disease states. Other differences between non-pathological and pathological 3D microenvironments may be biochemical in nature; for example, the 3D microenvironments in many disease states, such as cancer, may be hypoxic. Moreover, cells in many pathophysiologies release soluble factors into the 3D microenvironment that may affect other cells. Specifically, cancer-associated fibroblasts (CAFs) have been reported to release soluble factors, such as cytokines and exosomes [34]. In disease states, such as atherosclerosis—a CVD characterized by the presence of atherosclerotic plaque made up of oxLDL-laden foam cells underneath the endothelial monolayer in the arteries—similar cell behaviors occur [11]. Specifically, in atherosclerosis, endothelial cells may develop surface proteins, such as vascular cell adhesion molecule 1 and intercellular adhesion molecule 1, after biomechanical changes in their 3D microenvironment related to the flow of blood [35]. The surface proteins then allow the monocytes to attach to the endothelium, and the monocytes in the 3D atherosclerosis microenvironment are subjected to a variety of factors from the endothelial cells that result in the differentiation of monocytes into macrophages, which then become ox-LDL-laden foam cells, significantly contributing to disease progression [11, 35]. Therefore, the 3D microenvironment is relevant for *in vitro* high-throughput drug screening of disease models, especially for disease models of cancers and CVDs. However, many aspects of the 3D microenvironment are not adequately modeled in 2D *in vitro* models—for example, the 3D ECM [2]. A variety of 2D *in vitro* models have been developed, including 2D models with 3D characteristics, such as cells on tissue culture plastics coated with ECM-mimicking materials [36]. However, these 2D *in vitro* models were still only 2D models, which necessitated the development of 3D *in vitro* models.

3.2 The types of 3D in vitro models in high-throughput drug screening

The 3D *in vitro* models in the HTS studies discussed in this review—3D cell-laden scaffolds and hydrogels—have cells that are encapsulated in or surrounded by ECM-mimicking materials (Fig. 2). 3D cell-laden scaffolds and hydrogels of many different shapes have been used in the HTS studies discussed in this review, but cube- and sphere-shaped versions of these 3D models, which we define as 3D cell sheets and spheroids with ECM-mimicking components for the purposes of this review, have been especially popular for high-throughput drug screening. In addition, these models have been used to develop 3D *in vitro* microfluidic and organ-on-a-chip (OOC) models for HTS [37–39]. While cell sheet, spheroid, and microfluidic model systems have also been fabricated from 2D cell cultures instead of 3D cell-laden scaffolds or hydrogels, many of these models only include the ECMs of the cells in the model—they do not include an additional ECM-mimicking component—and, therefore, we have decided not to include them in this review [11, 40, 41]. In the following section, we will describe the types of 3D *in vitro* models in more detail and discuss recent studies in which 3D *in vitro* models of high-impact diseases—namely, cancers and CVDs—were demonstrated to be HTS-compatible. Please see Table I for an overview of the studies reviewed in the following section.

3.2.1 cell-laden scaffolds and hydrogels

The first type of 3D *in vitro* model we will discuss is a 3D cell-laden scaffold, a framework of natural or synthetic polymers, which is laden with cells [42]. Based on the general structure of a 3D cell-laden scaffold, it may be classified as either a fibrous (fiber) scaffold or a porous (pore) scaffold (Fig. 2) [43]. Recent HTS studies in which 3D *in vitro* cell-laden scaffolds have been used include studies from Yan et al. and Xin et al. [7, 44]. In the first study, Yan et al. described a poly-methyl methacrylate (PMMA) micro-scaffold array reminiscent of a 384-well microtiter plate, in which there were two stacked layers of 348 wells with an upper layer that had wells that were open at the bottom [7]. Gelatin hydrogels were prepared in the lower layer of wells by simple addition of a gelatin cryogel precursor followed by cryogelation. Complete lyophilization of the gelatin hydrogels was then performed to turn the gelatin hydrogels into gelatin micro-scaffolds, which were imaged with scanning electron microscopy. After UV-sterilization of the gelatin scaffolds, the upper layer of wells was stacked onto the lower layer to complete the micro-scaffold array chip, and a variety of cancer cells, such as colorectal and lung cancer cells, were added to the gelatin micro-scaffolds. The cancer cell-laden gelatin micro-scaffold 3D *in vitro* models and 2D *in vitro* cancer cell models were then treated with 12 chemotherapeutics, and cytotoxicity was determined experimentally with the CellTiter-Blue® assay—one of the Resazurin HTS assays—and a microplate reader [7, 17]. In addition, live/dead HTS assay reagents, calcein AM and PI, were used with a high-content imaging system, which is a high-throughput, microtiter plate-compatible imaging system [7, 45]. Cytotoxicity of several chemotherapeutics was diminished in the 3D cell-laden scaffolds relative to the 2D models [7]. Interestingly, cytotoxicity of the two chemotherapeutics with high efficacy in the 2D models—gemcitabine and vinorelbine—and a chemotherapeutic effective in both the 2D and 3D models—doxorubicin—were then evaluated *in vivo* in a lung cancer xenograft mouse model. Unsurprisingly, doxorubicin was significantly more effective than gemcitabine and vinorelbine as determined by the size of the tumors in the mouse model. Moreover, the effects of gemcitabine and vinorelbine on the tumors were indistinguishable, statistically, from that of phosphate-buffered saline, the control.

3D *in vitro* cancer cell-laden scaffolds have also been used in recent HTS studies to determine the ability of chemotherapeutics to regulate the expression of specific proteins, such as survivin—a protein that may be associated with cancer cell behaviors, such as chemoresistance [44, 46]. In one such study from Xin et al., genetically-modified MCF-7 breast cancer cells, in which expression of enhanced GFP (EGFP) was proportional to that of survivin, were seeded on polyethylene terephthalate (PET) scaffolds in 3×3 arrays of interconnected wells in a 384-well microtiter plate [44]. A microplate reader was then used to determine the fluorescence of the cancer cell-laden scaffold and the non-scaffold wells in each 3×3 array and, thus, provide a quantitative value for relative survivin expression in the cancer cells. Next, an HTS experiment was performed with two chemotherapeutics—doxorubicin and cisplatin—and the genetically-modified MCF-7 breast cancer cell-laden PET scaffolds to determine if these chemotherapeutics alter the survivin expression in cancer cells. A second line of EGFP MCF-7 breast cancer cells was used as a control to account for the loss of EGFP fluorescence associated with chemotherapeutic-induced cell death. This study revealed that doxorubicin and cisplatin were cytotoxic in the 3D *in vitro* breast cancer cell-laden scaffold model, and doxorubicin was able to suppress the expression of survivin in this model.

The second type of 3D *in vitro* model we will discuss is a cell-laden hydrogel. Like the 3D cell-laden scaffolds, 3D cell-laden hydrogels have natural or synthetic polymers; in hydrogels, these polymers are crosslinked to form a hydrophilic 3D polymer network, in which water is

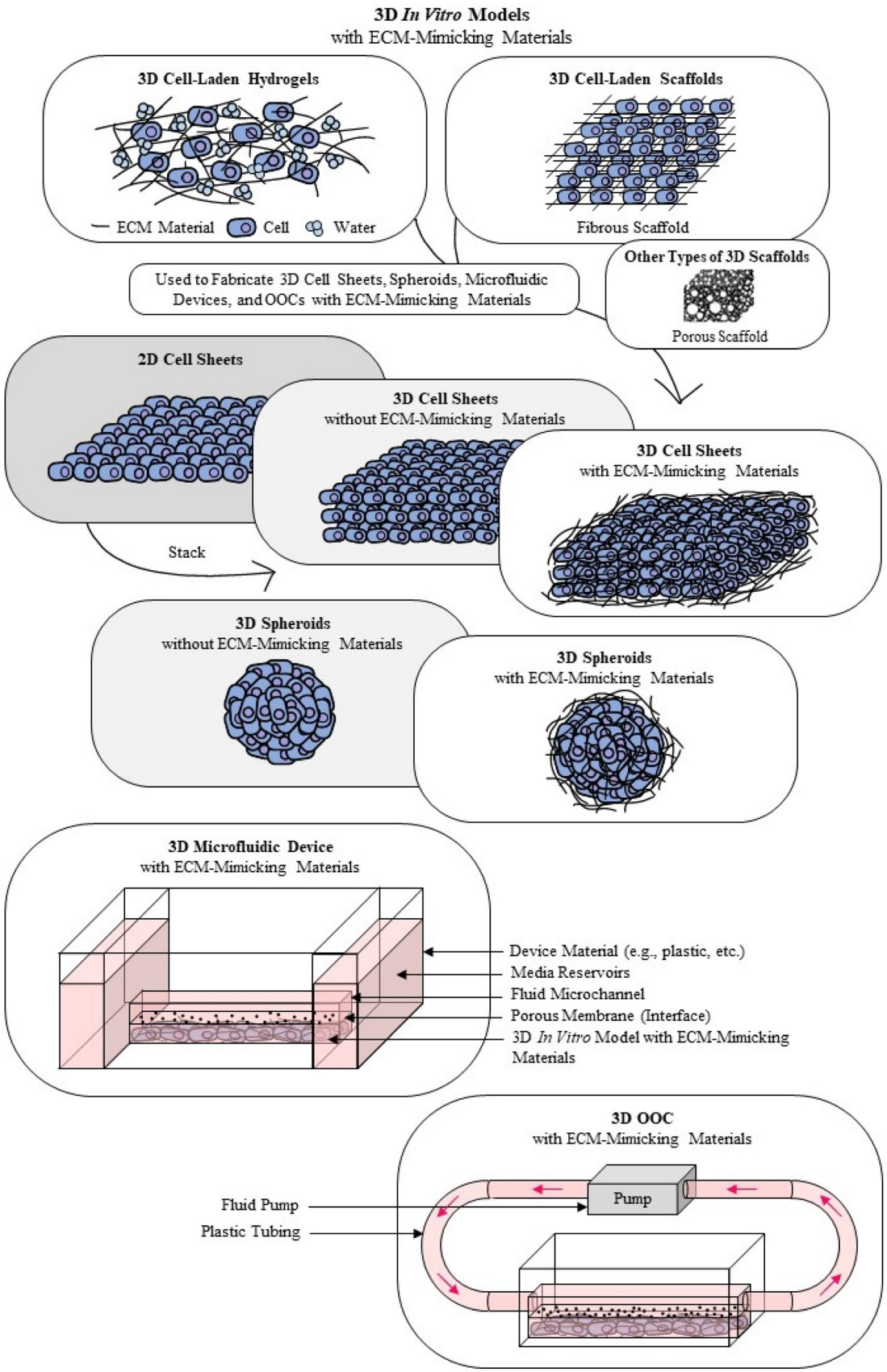
3D *In Vitro* Models
with ECM-Mimicking Materials
3D Cell-Laden Hydrogels
ECM Material
Cell
Water
3D Cell-Laden Scaffolds
Fibrous Scaffold
Other Types of 3D Scaffolds
Porous Scaffold
Used to Fabricate 3D Cell Sheets, Spheroids, Microfluidic Devices, and OOCs with ECM-Mimicking Materials
2D Cell Sheets
3D Cell Sheets
without ECM-Mimicking Materials
3D Cell Sheets
with ECM-Mimicking Materials
Stack
3D Spheroids
without ECM-Mimicking Materials
3D Spheroids
with ECM-Mimicking Materials
3D Microfluidic Device
with ECM-Mimicking Materials
Device Material (e.g., plastic, etc.)
Media Reservoirs
Fluid Microchannel
Porous Membrane (Interface)
3D *In Vitro* Model with ECM-Mimicking Materials
3D OOC
with ECM-Mimicking Materials
Fluid Pump
Plastic Tubing
Pump

◀**Fig. 2** Types of 3D *In vitro* Models. An overview of 3D *in vitro* models. In this review, we use the term "3D *in vitro* model" to refer to any *in vitro* model system, in which the cells of the model are surrounded or encapsulated in three dimensions by ECM-mimicking materials. Specifically, 3D *in vitro* models include 3D cell-laden hydrogels and scaffolds as well as the various types of 3D models that may be fabricated from cell-laden hydrogels and scaffolds, such as 3D cell sheets, spheroids, and microfluidic and OOC systems. The microfluidic and OOC systems depicted here are general examples based on the L-TumorChip OOC reviewed in Sect. 3.2.4 [39]. For an image of a 3D cell-laden hydrogel, please see Fig. 3. In addition, for images of 3D cell-laden hydrogel-based cell sheets, spheroids, and microfluidic systems, please see Fig. 4, Fig. 5, and Fig. 6, respectively. Readers are directed to Fig. 1A from Yan et al. for an image of a 3D cell-laden scaffold [7]

retained [47, 48]. A recent cancer HTS study, in which a cell-laden hydrogel was used, was reported by Lee et al. [49]. In this study, the 3D *in vitro* cell laden hydrogel models were composed of breast cancer cells encapsulated in alginate hydrogels on the pillars of 384-pillar microtiter plate (Fig. 3A, B). These 3D *in vitro* models were fabricated in high-throughput with an automated liquid handling system, after which the 384-pillar plate was overturned and stacked onto a 384-well microtiter plate with cell culture medium, such that the 3D cell-laden hydrogels on the pillars were submerged in the medium. The 3D cell-laden hydrogels were later submerged in the two 384-well microtiter plates with chemotherapeutics and the live/dead HTS assay reagent, calcein AM, respectively. Next, the calcein AM-stained cancer cell-laden hydrogels were imaged with a high-content imaging system, and fluorescence, which was representative of relative cell viability, was determined. Results for this study were similar to the results of the other HTS cancer studies discussed thus far—namely, elevated chemotherapeutic resistance in the cancer cells of the 3D model relative to the 2D model was indicated (Fig. 3C) [44, 49]. Recent cardiovascular HTS studies in which 3D *in vitro* cell-laden hydrogels were used include Ma et al. [50]. In this study, the 3D models were induced pluripotent stem cell–derived cardiomyocyte (iPSC-CM)-laden type I collagen and fibrin hydrogels in a 96-well microtiter plate, in which poly (ethylene glycol) diacrylate (PEGDA) micro-pillar force gauges were 3D printed. Because the iPSC-CMs in the cell-laden hydrogel were able to bend the PEGDA micro-pillar force gauges, which was visualized with a microscope, the force in micronewtons of the iPSC-CMs on the pillars could be determined in this study. Amazingly, the amplification of this force by the cardiovascular drugs isoproterenol, levosimendan, and omecamtiv mecarbil could be appreciated in this 3D *in vitro* model.

3.2.2 Cell sheets

The 3D *in vitro* cell sheet models we will discuss in this section are 3D cell sheet models that have been developed

Table I An overview of the 3D HTS assay studies discussed in this review. Readers are directed to the referenced papers for more detailed information about the studies

3D HTS study	3D *in vitro* model	Measurement system	Disease model	Property assayed	Ref.
Yan et al	Cell-laden scaffold	Microplate reader; high-content imaging system	Colorectal and lung cancer	Cytotoxicity	[7]
Xin et al	Cell-laden scaffold	Microplate reader	Breast cancer	Survivin expression	[44]
Lee et al	Cell-laden hydrogel	High-content imaging system	Breast cancer	Cytotoxicity	[49]
Ma et al	Cell-laden hydrogel	Microscopy	Cardiovascular disease	Force	[50]
Lee et al	Cell sheet	Microplate reader, fluorescence microscopy	Epithelial cancer	Cytotoxicity	[51]
Chitty et al	Cell sheet	Microscopy	Pancreatic cancer	Invasion	[53]
Puls et al	Spheroid	High-content imaging system	Pancreatic cancer	Invasion	[58]
Cutrona and Simpson	Spheroid	High-content imaging system	Colorectal cancer	NP infiltration	[29]
Park et al	Microfluidic device	Fluorescence microscopy	Cancer	Cytotoxicity	[37]
Yu et al	Microfluidic device	Fluorescence microscopy	Colorectal cancer	Angiogenesis	[38]
Chi et al	Organ-on-a-chip	Fluorescence microscopy	Breast cancer	Protein expression, invasion, and cytotoxicity	[39]

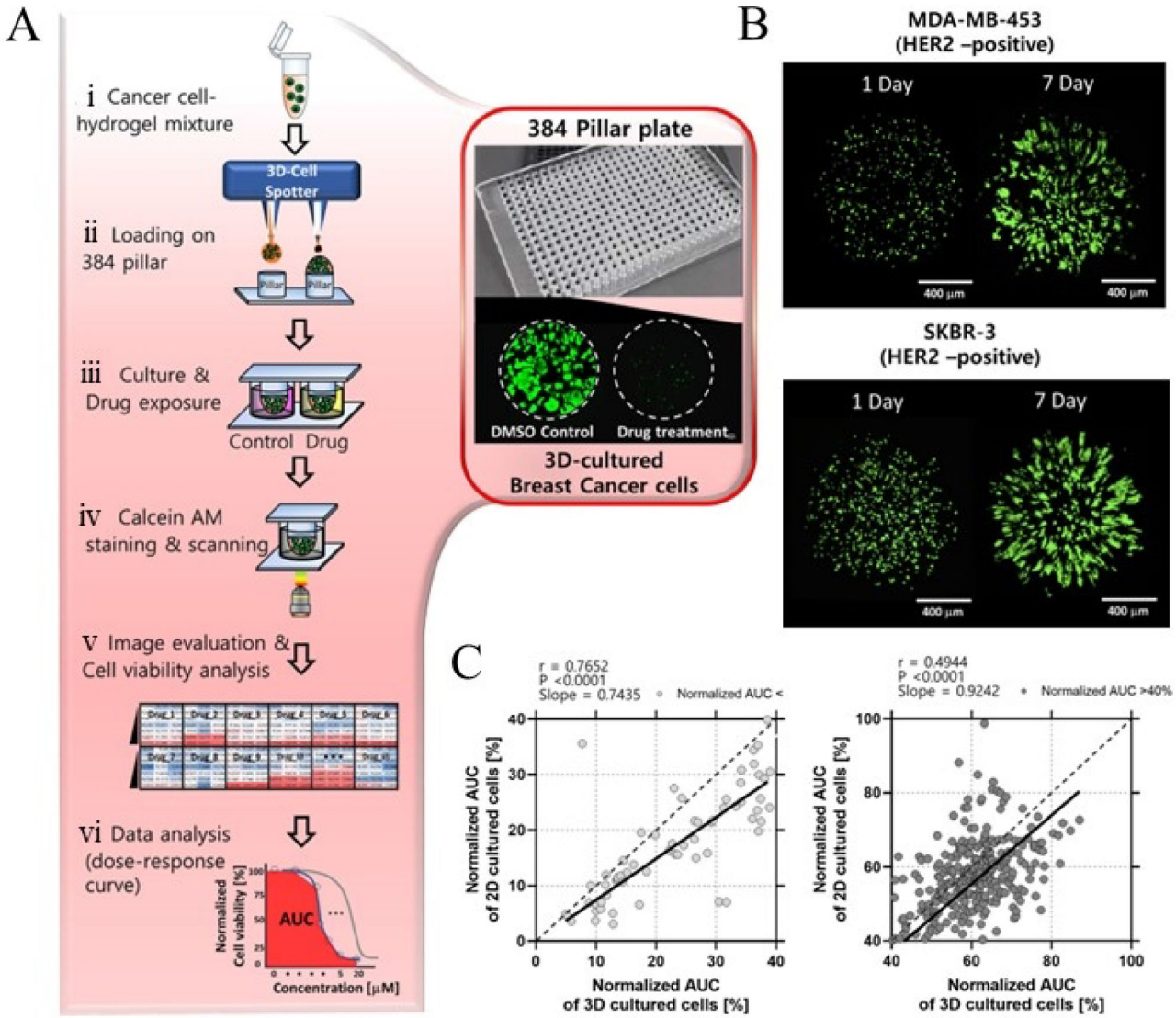

Fig. 3 HTS Assay with a 3D *In vitro* Cell-Laden Hydrogel Model. **A** The high-throughput fabrication scheme for the 3D *in vitro* breast cancer cell-laden hydrogels from the study by Lee et al. [49]. **B** Images of the calcein AM-stained cell-laden hydrogels for two breast cancer cell lines—MDA-MB-453 and SKBR-3. **C** Relative cell viability of the breast cancer cell-laden hydrogels after treatment with a chemotherapeutic was determined. A measure of the relative viability was then plotted against that of the 2D breast cancer cell model—breast cancer cells in a 384-well microtiter plate. Adapted with permission from [49]

with sheet-shaped 3D cell-laden scaffolds or hydrogels. There are also 2D cell sheet models—monolayers of cells on polymers, such as poly(N-isoproplyacrylamide) (PAAm), which can be separated from the cell sheet [40]. In addition, multiple layers of 2D cell sheets have been stacked for 3D cell sheet models. However, we have decided not to include these 3D cell sheet models in this review as this type of 3D model does not have an additional ECM-mimicking component. To our knowledge, no 3D *in vitro* cell sheet models of CVDs meeting this definition have been used for high-throughput cardiovascular drug screening other than our own recently-developed 3D cell sheet-based atherosclerotic vascular tissue model, and there have only been a few for cancer-related drug screening applications. One such 3D model—a 3D oral fibroblast-laden fibrin hydrogel sheet—was the focus of a study from Lee et al. [51]. Epithelial cancer cell spheroids—sphere-shaped aggregates of cells without an ECM-mimicking component—or epithelial cancer cell and CAF co-culture spheroids and a 2D oral keratinocyte cell sheet were combined with this 3D cell sheet model to represent the metastasis of epithelial cancer to oral tissue (Fig. 4A).

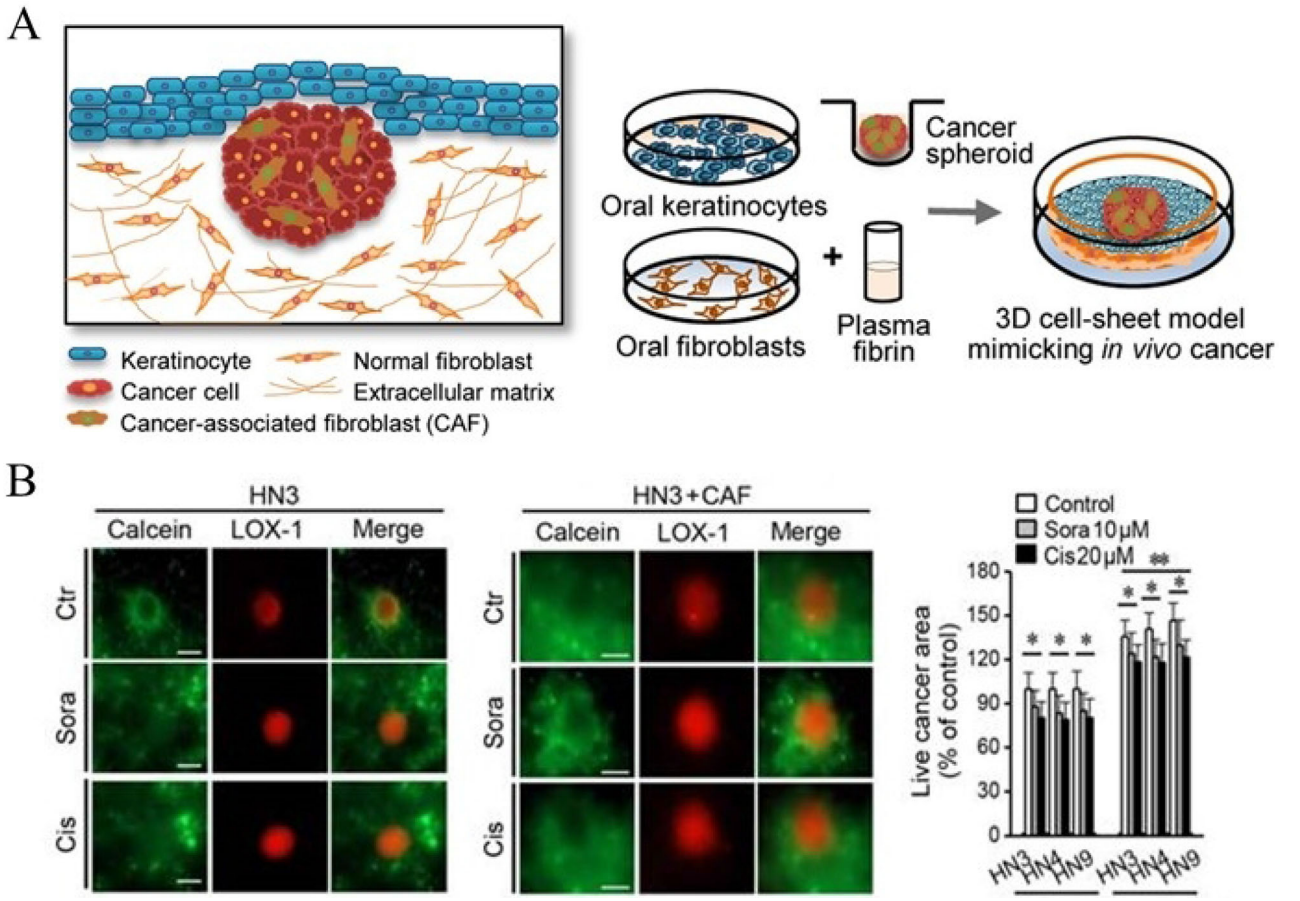

Fig. 4 HTS Assay with a 3D *In vitro* Cell Sheet Model. **A** The fabrication scheme for the 3D *in vitro* cell sheet model of oral tissue and metastasized epithelial cancer from Lee et al. [51]. **B** Images of the 3D *in vitro* cell sheet model after application of the chemotherapeutics, sorafenib and cisplatin, and HTS-compatible live/dead assay reagents, calcein AM and PI. Adapted with permission from [51]

Cytotoxicity of cisplatin and sorafenib for the epithelial cancer cells in the 3D cell sheet was then quantified with two methods—the first of which was the Cell Counting Kit-8 (CCK-8) assay, a type of metabolic HTS assay similar to the MTT assay [51, 52]. The second method by which cytotoxicity was quantified was with fluorescence microscopy of calcein AM and PI [51]. Another fluorescent stain LOX-1 was also used to quantify hypoxia. Interestingly, the results of these experiments did not support the hypothesis that CAFs would have a protective effect against chemotherapeutics in the 3D sheet epithelial cancer cell and CAF co-cultures. However, the invasive character of the co-cultures, as quantified by the area of calcein AM-stained epithelial cancer cells, was elevated relative to that of the epithelial cell monocultures in the 3D cell sheet model (Fig. 4B).

Similar 3D *in vitro* cell sheet models for cancer-related high-throughput drug screening, such as the Mini-Organo, have also been used in recent studies [53]. For example, in one such study reported by Chitty et al., Mini-Organos—3D cell sheets composed of CAFs encapsulated in collagen hydrogel onto which cancer cells were cultured—were fabricated in a bovine serum albumin-coated 96-well microtiter plate. Although the authors characterized this model as high-throughput, the cancer cell invasion assay they performed required several low-throughput steps. Specifically, the 3D cell sheets were harvested individually with forceps for the invasion assay, which was conducted in a 6-well plate format. After the invasion assay, the 3D cell sheets were harvested, fixed, sectioned, stained, and viewed with a microscope to assign the cancer cells a numerical value for invasive index—the percent of cancer cells that successfully penetrated the 3D cell sheet. Results of a preliminary study validated this invasion assay—specifically, this study demonstrated that the statin, blebbistatin, significantly reduced the invasive character of the Pdx1-Cre line of pancreatic ductal adenocarcinoma (PDAC) cells.

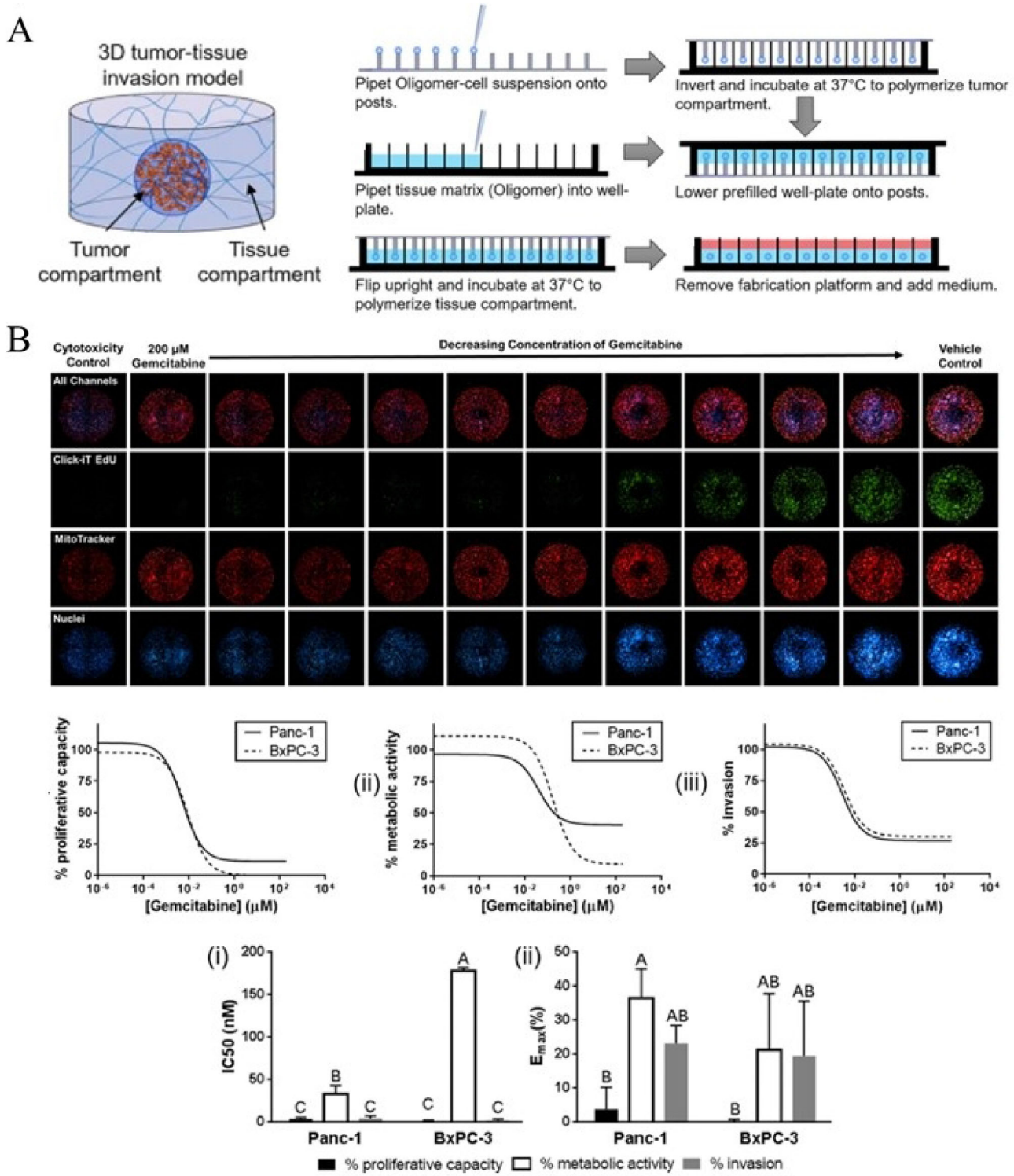

Fig. 5 HTS Assay with a 3D *In vitro* Spheroid Model. **A** The high-throughput fabrication scheme for the 3D *in vitro* PDAC spheroid models from Puls et al. [58]. **B** Click-iT EdU 488 and MitoTracker Red were applied to the 3D models, which were imaged with a high-content imaging system. Fluorescent images from the red and green fluorescence channels, with which relative cell viability, proliferation, and invasive character of BxPC-3 and Panc-1 PDAC cells were determined. Adapted with permission from [58]

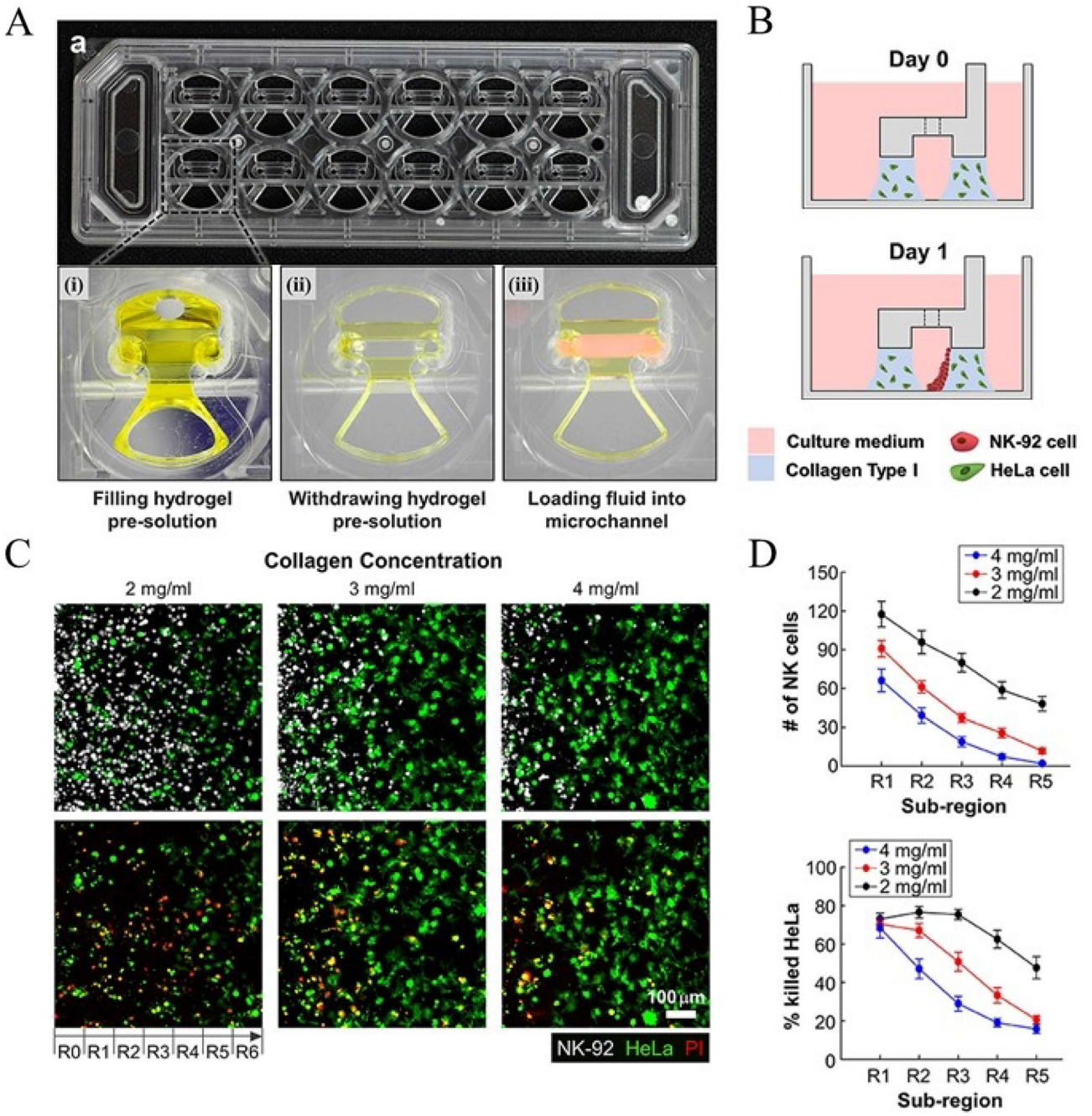

Fig. 6 HTS Assay with a 3D *In vitro* Microfluidic Model. **A** The CACI-IMPACT microfluidic device from Park et al. [37]. **B** A scheme for the 3D *in vitro* model: two cancer cell-laden collagen hydrogels and NK cells preferentially-adhered to one of the hydrogels. **C** Images of the cancer cell-laden hydrogels and natural killer cells, which are associated with green and far-red fluorescence, respectively. Red fluorescence was associated with PI. **D** Green, red, and far-red fluorescence was used to quantify invasion of the NK-92 cells into the cancer-cell laden hydrogels as well as NK-92-mediated cell death. Adapted with permission from [37]

3.2.3 Spheroids

The 3D *in vitro* spheroid models we will discuss in this section are 3D spheroid models that have been developed with sphere-shaped 3D cell-laden scaffolds or hydrogels. While there are other versions of 3D spheroids—namely, spheroids, or sphere-shaped aggregates of cells without an additional ECM-mimicking component, which have been fabricated in the past from 2D cell sheets or from cell culture under low adhesion conditions—we have decided

not to include them in this review as this type of 3D model does not have an ECM-mimicking component [54, 55]. 3D spheroid models appear to have been used most often for cancer-related high-throughput drug screening. However, there are 3D *in vitro* spheroid models for CVDs—the most notable of which is a spheroid model for atherosclerotic plaque from Nguyen et al. and Rakshit et al. [11, 56, 57]. Unfortunately, this spheroid model did not include an ECM-mimicking component, thus it will not be reviewed here. In contrast, there are several excellent examples of studies in which 3D *in vitro* cancer spheroid models have been used for HTS, such as that presented by Puls et al. [58]. In this HTS study, the 3D spheroid models were sphere-shaped type I collagen oligomer hydrogels, in which pancreatic cancer cells were encapsulated, on a 3D printed 96-well pillar plate (Fig. 5A). After polymerization of the cell-laden hydrogels, the pillar plate was submerged in a 96-well microtiter plate with type I collagen oligomer hydrogels. Cell culture medium, drugs, and HTS reagents were then applied to the 3D *in vitro* model—the 3D model was small enough that the microtiter plate wells could still be used as fluid reservoirs. Specifically, the HTS-compatible reagents, Click-iT Edu 488 and MitoTracker Red, and the nuclear stain, Hoechst 33,342, were applied to the 3D models, which were imaged with a high-content imaging system (Fig. 5B). Because the Click-iT EdU and MitoTracker reagents were not included in our previous discussion of common 2D HTS assay reagents, they will be briefly described here. MitoTracker is a positively-charged fluorescent compound that is driven into the mitochondrial matrix in viable cells by the electrochemical concentration gradient [59]. Conversely, 5-ethynyl-2′-deoxyuridine (EdU) is a 2′-deoxyuridine nucleoside to which an alkyne group has been added [60, 61]. EdU is supplied to *in vitro* models, which are later treated with copper(I) and an azide-modified fluorescent dye; the azide of the fluorescent dye interacts with the alkyne of the EdU in the DNA of the *in vitro* model to fluorescently stain the nucleoside. In the study from Puls et al., these HTS assays revealed that the chemotherapeutic gemcitabine failed to suppress the invasive character of BxPC03 and Panc-1 cells despite suppressing proliferation of these cells [58]. Based on these results, high-throughput drug screens for cancers may need to evaluate the effects of chemotherapeutics on the invasive character of cancer cells in addition to standard *in vitro* cytotoxicity determinations.

Other studies have also demonstrated the use of high-content imaging systems for 3D HTS assays with spheroid *in vitro* models; for example, in a study from Cutrona et al., colorectal cancer cell spheroids were fabricated in high throughput in a Matrigel-coated 96-well microtiter plate [29]. Later, the Matrigel was extracted chemically, and the force of gravity dragged the spheroids down, such that more spheroids were in the same focal plane for imaging with a high-content imaging system. Using this protocol, the authors determined the degree to which the 3D *in vitro* spheroid models were infiltrated by fluorescent NPs as well as the influence of potential therapeutics, such as small interfering RNAs (siRNAs), on this infiltration. Specifically, several siRNAs significantly limited the appearance of NPs within the cancer spheroids—most notably, siCLTC, siRAB7A, and siRAB33B. This type of high-throughput drug screening study may be of interest to those studying CVDs. 2D HTS studies for atherosclerosis, specifically, have involved the high-throughput evaluation of the cellular uptake of particles, such as the uptake of oxLDL by macrophages to become foam cells as was studied in 2D in Etzion et al. [21]. However, to our knowledge, there are no suitable 3D models of atherosclerosis for high-throughput drug screening of this nature.

3.2.4 Microfluidic and OOC systems

The microfluidic devices or chips reviewed in this paper are composed of three components: (1) a part of the microfluidic device in which an *in vitro* model is cultured, (2) one or more fluid reservoirs with microchannels through which cell culture medium may flow to and from the *in vitro* model, and (3) one or more parts of the microfluidic device in which the *in vitro* model interfaces with the fluid-filled microchannels [37–39]. While the *in vitro* models within the microfluidic chips discussed here are 3D *in vitro* models, 2D *in vitro* models may also be cultured in microfluidic chips, leading to 2D or 3D microfluidic systems, respectively [11]. Advanced, tissue-engineered *in vitro* models in microfluidic systems, such as the *L*-TumorChip from the study by Chi et al., are sometimes referred to as OOCs [39, 62]. This microfluidic device, the *L-TumorChip*, incorporates a fourth component: (4) a mechanism by which to drive fluid through the system and, thus, expose the cells of the *in vitro* model in the microfluidic chip, to biomimetic forces, such as shear fluid flow [39]. When used as a platform for 3D *in vitro* models, microfluidic chips have seen success in high throughput drug screening applications as demonstrated by several studies such as those from Park et al., Yu et al., and Chi et al. [37–39].

In the first study reported by Park et al., the microfluidic device was the cytotoxicity assay for cancer immunotherapy injection molded plastic array culture (CACI-IMPACT)—a 2 × 6 array of polystyrene (PS) wells, in which chair-shaped PS inserts were suspended (Fig. 6A) [37]. The 3D *in vitro* models used with this microfluidic device were fluorescently-tagged 3D cancer cell-laden type I collagen hydrogels, which were manually pipetted into

the CACI-IMPACT device followed by an incubation period, which allowed the hydrogels to set. After the 3D *in vitro* models were fabricated within the high-throughput CACI-IMPACT microfluidic device, fluorescently-tagged natural killer (NK)-92 cells were injected between the 3D cell-laden hydrogels and the device was briefly rested on its side, so that the NK-92 cells adhered preferentially to one of the two cell-laden hydrogels in each well (Fig. 6B). The hydrogels were later perfused with the HTS assay reagent PI and imaged at 26 tissue depths, each 4 μm apart (Fig. 6C). Fluorescence from the channel associated with the NK-92 cells—far-red fluorescence—was used to quantify invasion of the NK-92 cells into the cancer-cell laden hydrogels (Fig. 6D). Chemotherapeutic potential of the NK-92 s was similarly quantified with fluorescence from the channel associated with the cancer cells and PI—green and red, respectively. The fluorescent images revealed an inversely proportional relationship between the concentration of type I collagen in the cancer cell-laden hydrogels and NK-92 cell-mediated cancer cell death, which was most likely caused by the additional collagen molecules in the hydrogel impeding the NK-92 cells. Importantly, this result highlights a crucial difference between 2 and 3D *in vitro* models and may help to explain differences between the results of 2D and 3D cancer-related drug screening studies.

A slightly-modified version of the CACI-IMPACT device was also used in a more recent study from Yu et al. [38]. In this study, the 3D microfluidic device, the Microvascular IMPACT (MV-IMPACT), was miniaturized relative to the CACI-IMPACT [37, 38]. Specifically, the well inserts were redesigned so that three hydrogels could be fabricated in each group of two interconnected 384-well microtiter plate wells. The hydrogels in the middle of the wells in this device were fibrin hydrogels, which were bordered on one side by endothelial cells and on the other side by fibroblast-laden fibrin hydrogels [38]. Images of fluorescently-labeled endothelial cells at different imaging depths in the fibrin hydrogel were then used to ascribe the fibroblasts a numeric value for pro-angiogenic character. A high-throughput drug screening experiment was also performed with gamma-secretase and Notch inhibitor DAPT-supplemented cell culture medium. As a result of this study, DAPT was discovered to induce branching in the 3D *in vitro* angiogenesis model as well as other geometric characteristics, such as increased vessel width. Perhaps this 3D HTS assay will be further developed for vascular- or cardiovascular-related high-throughput drug screening. However, in this study, the 3D HTS assay was then used to determine the difference in pro-angiogenic character between cultures of fibroblasts and co-cultures of fibroblasts and cancer cells. Notably, the co-culture of fibroblasts and one colorectal cancer cell line, SW620, significantly outperformed the monoculture of SW620 cells, highlighting the importance of including multiple cell lines in 3D *in vitro* models, especially 3D *in vitro* disease models used for high-throughput drug screening. Although the co-cultured fibroblasts and cancer cells in this 3D *in vitro* model were not used for drug screening, cancer-related high-throughput drug screening could have easily been performed as in the DAPT experiment.

In the last study from Chi et al., the authors used a 3D *in vitro* OOC model for high-throughput drug screening [39]. In this study, the 3D OOC model was the *L*-TumorChip, an advanced triple-negative breast cancer (TNBC) model. The *L*-TumorChip, like other 3D OOCs, was a 3D *in vitro* model in a microfluidic device. Specifically, the 3D model was an MDA-MB-231 breast cancer cell and fibroblast-laden Matrigel hydrogel. The microfluidic device had a small space in which the cell-laden hydrogel could be fabricated, over which there was a thin layer of perforated polydimethylsiloxane. On the other side of this, there was a human microvascular endothelial cell (HMVEC)-lined microchannel for syringe pump-driven fluid flow over the cell-laden hydrogel. Multiple aspects of the 3D cancer cell and fibroblast-laden hydrogels and the associated HMVECs, such as the permeability of the HMVECs, were then assayed. For this experiment, 10 kDa FITC-dextran and 70 kDa Texas Red-dextran were added to the cell culture media driven through the microchannel. Green and red fluorescence in the cell-laden hydrogel, which was associated with the passage of the smaller FITC-dextran and the larger Texas Red-dextran, respectively, through gaps in the HMVEC monolayer, was then quantified with a fluorescent microscope. In addition, the invasive character of the TNBC cells in the 3D cell-laden hydrogel was quantified similarly; red fluorescence associated with RFP-MDA-MB-231 cells could be detected in the fluid microchannel of the *L*-TumorChip as early as one-week post-initiation of the experiment. Thus, the *L*-TumorChip may serve as the foundation for cancer-related drug screening studies, including high-throughput drug screening studies for chemotherapeutics, such as doxorubicin. In this study, the cytotoxicity of doxorubicin was quantified with a caspase-3 HTS assay, in which a DNA stain is applied that only fluoresces after caspase 3/7 acts on it [39, 63]. Doxorubicin cytotoxicity, as quantified with a fluorescent microscope, was shown to vary with the cells in the cell-laden hydrogel [39]. Interestingly, in this study, CAFs were protective against doxorubicin in MDA-MB-231 co-cultures [39]. Parrish et al. also reported a similar cancer-related high-throughput drug screening study with a 3D *in vitro* OOC model [64].

4 Conclusions and future perspectives

The use of 3D *in vitro* models in high-throughput drug screening for high-impact diseases, such as cancer and CVDs, has grown increasingly feasible as evidenced by the 3D HTS studies discussed in this review, which are summarized in Table I. While there are significant challenges associated with using 3D *in vitro* models in high-throughput drug screening, many advances have been made in recent years. Specifically, challenges associated with the (1) high-throughput fabrication of 3D *in vitro* models and the (2) compatibility of 3D *in vitro* models with HTS assays have been addressed. Indeed, 3D cell-laden hydrogels may now be fabricated in microtiter plates in a high-throughput manner with automated liquid handling systems, and there are several methods by which 3D cell-laden hydrogels may be fabricated in microfluidic devices [37, 38, 49]. Additionally, acoustics has been leveraged to make cancer cell-laden gelatin methacryloyl hydrogels in microfluidic devices for high-throughput drug screening [65]. Likewise, high-throughput 3D bioprinters have been developed with which cell-laden scaffolds can be 3D printed into 96-well microtiter plates [66]. Furthermore, the development of high-content imaging systems as well as protocols, such as that presented by Cutrona et al., have allowed HTS assays that were previously incompatible with 3D *in vitro* models to be used [29]. In addition, histology-based 3D HTS assays may now be performed with the use of technology, such as the 4D-printed transformable tube array from Yang et al. with which 3D *in vitro* models in microtiter plates can be moved to histological cassettes, stained, sectioned, and imaged in high throughput [67].

While cancers and CVDs are both high-impact diseases, cancer-related 3D high-throughput drug screening studies vastly outnumber CVD-related 3D high-throughput drug screening studies. Furthermore, our literature search uncovered only a handful of recent CVD-related HTS studies that used 3D *in vitro* models with ECM-mimicking components. Moreover, several types of 3D *in vitro* models with ECM-mimicking components, such as 3D *in vitro* cell sheet models, have not yet, to our knowledge, been used for CVD-related high-throughput drug screening, recently or otherwise. Therefore, there is a significant need to develop 3D models with ECM-mimicking components for CVDs, such as atherosclerosis, that are amenable to high-throughput fabrication schemes and HTS assays. Meanwhile, there is room for improvement in many current cancer-related 3D HTS assays, as demonstrated by the frequency with which low-throughput measurement systems, such as fluorescence microscopes, were used in the 3D HTS studies we reviewed (Table I). Additionally, as shown in Table 1, many of the 3D HTS assays discussed in this review are severely limited in that they are only designed to assay cytotoxicity. This is in contrast to more complicated but innovative and useful 3D HTS assays, such as the 3D HTS assays presented in the studies from Cutrona et al. and Ma et al., which were able to assay the 3D *in vitro* models for characteristics relevant for cancer and CVD drug screening, such as cardiac cell contraction and infiltration of therapeutics into 3D *in vitro* models [29, 50]. However, with the technological advances discussed in this review, we fully expect many additional 3D HTS assays of this nature to be developed in the future.

Acknowledgment Funding was provided by National Heart, Lung, and Blood Institute (Grant No. R01HL163802).

Conflict of interest The authors have no financial conflicts of interest.

Ethical statement There are no animal experiment carried out for this article

References

1. Congressional Budget Office. Research and development in the pharmaceutical industry. 2021. https://www.cbo.gov/publication/57025.
2. Astashkina A, Mann B, Grainger DW. A critical evaluation of in vitro cell culture models for high-throughput drug screening and toxicity. Pharmacol Ther. 2012;134:82–106.
3. Joseph SJ, Malindisa ST, Ntwasa M. Two-dimensional (2D) and three-dimensional (3D) cell culturing in drug discovery. In: Cell culture. Mehanna RA, editor. IntechOpen. https://doi.org/10.5772/intechopen.81552
4. Langhans SA. Three-dimensional in vitro cell culture models in drug discovery and drug repositioning. Front Pharmacol. 2018;9:6.
5. Jansen KA, Donato DM, Balcioglu HE, Schmidt T, Danen EH, Koenderink GH. A guide to mechanobiology: where biology and physics meet. Biochim Biophys Acta 2015;1853:3043–52.
6. Nam KH, Smith AS, Lone S, Kwon S, Kim DH. Biomimetic 3D tissue models for advanced high-throughput drug screening. J Lab Autom. 2015;20:201–15.
7. Yan X, Zhou L, Wu Z, Wang X, Chen X, Yang F, et al. High throughput scaffold-based 3D micro-tumor array for efficient drug screening and chemosensitivity testing. Biomaterials. 2019;198:167–79.
8. Somarathna M, Hwang PT, Millican RC, Alexander GC, Isayeva-Waldrop T, Sherwood JA, et al. Nitric oxide releasing nanomatrix gel treatment inhibits venous intimal hyperplasia and improves vascular remodeling in a rodent arteriovenous fistula. Biomaterials. 2022;280:121254.
9. Andukuri A, Minor WP, Kushwaha M, Anderson JM, Jun HW. Effect of endothelium mimicking self-assembled nanomatrices on cell adhesion and spreading of human endothelial cells and smooth muscle cells. Nanomedicine. 2010;6:289–97.
10. Ramaiahgari SC, den Braver MW, Herpers B, Terpstra V, Commandeur JN, van de Water B, et al. A 3D in vitro model of differentiated HepG2 cell spheroids with improved liver-like properties for repeated dose high-throughput toxicity studies. Arch Toxicol. 2014;88:1083–95.

11. Chen J, Zhang X, Millican R, Lynd T, Gangasani M, Malhotra S, et al. Recent progress in in vitro models for atherosclerosis studies. Front Cardiovasc Med. 2022;8:790529.
12. Attene-Ramos MS, Austin CP, Xia M. High throughput screening. In: Encyclopedia of toxicology. 3rd ed. Wexler P, editor. Academic Press; 2014. pp. 916–7.
13. Wildey MJ, Haunso A, Tudor M, Webb M, Connick JH. High-throughput screening. In: Annual reports in medicinal chemistry. Goodnow RA, editor. Academic Press; 2017. pp. 149–95.
14. Szymański P, Markowicz M, Olasik EM. Adaptation of high-throughput screening in drug discovery—toxicological screening tests. Int J Mol Sci. 2012;13:427–52.
15. Blay V, Tolani B, Ho SP, Arkin MR. High-throughput screening: today's biochemical and cell-based approaches. Drug Discov Today. 2020;25:1807–21.
16. Etzion Y, Muslin AJ. The application of phenotypic high-throughput screening techniques to cardiovascular research. Trends Cardiovasc Med. 2009;19:207–12.
17. Riss TL, Moravec RA, Niles AL, Duellman S, Benink HA, Worzella TJ, et al. Cell viability assays. In: Assay guidance manual [Internet] Markossian S, Grossman A, Brimacombe K et al., editors. Bethesda (MD): Eli Lilly & company and the national center for advancing translational sciences; 2004.
18. Ghasemi M, Turnbull T, Sebastian S, Kempson I. The MTT assay: utility, limitations, pitfalls, and interpretation in bulk and single-cell analysis. Int J Mol Sci. 2021;22:12827.
19. Rampersad SN. Multiple applications of alamar blue as an indicator of metabolic function and cellular health in cell viability bioassays. Sensors (Basel). 2012;12:12347–60.
20. Invitrogen. Viability and Cytotoxicity Assay Reagents—Section 15.2. In: The molecular probes handbook. ThermoFisher Scientific. https://www.thermofisher.com/us/en/home/references/molecular-probes-the-handbook/assays-for-cell-viability-proliferation-and-function/viability-and-cytotoxicity-assay-reagents.html. Accessed 28 Nov 2022.
21. Etzion Y, Hackett A, Proctor BM, Ren J, Nolan B, Ellenberger T, et al. An unbiased chemical biology screen identifies agents that modulate uptake of oxidized ldl by macrophages. Circ Res. 2009;105:148–57.
22. Invitrogen. Assays for cell enumeration, cell proliferation and cell cycle—Section 15.4. In: The molecular probes handbook. Thermofisher scientific. https://www.thermofisher.com/us/en/home/references/molecular-probes-the-handbook/assays-for-cell-viability-proliferation-and-function/assays-for-cell-enumeration-cell-proliferation-and-cell-cycle.html. Accessed 28 Nov 2022.
23. Anantanawat K, Pitsch N, Fromont C, Janitz C. High-throughput Quant-iT picogreen assay using an automated liquid handling system. Biotechniques. 2019;66:290–4.
24. Singer VL, Jones LJ, Yue ST, Haugland RP. Characterization of picogreen reagent and development of a fluorescence-based solution assay for double-stranded dna quantitation. Anal Biochem. 1997;249:228–38.
25. Chiba T, Tsuchiya T, Mori R, Shimokawa I. Protein reporter bioassay systems for the phenotypic screening of candidate drugs: a mouse platform for anti-aging drug screening. Sensors (Basel). 2012;12:1648–56.
26. Promega. reporter genes and their applications. https://www.promega.com/resources/guides/cell-biology/bioluminescent-reporters/. Accessed 28 Nov 2022.
27. Dobbs M, Hughes D, Narahari J, Choi J, Los G, Webb B, et al. Performing dual-spectral luciferase assays using the BMG Labtech POLARstar Omega plate reader. Thermofisher scientific. 2013. https://www.thermofisher.com/us/en/home/life-science/protein-biology/protein-biology-learning-center/protein-biology-resource-library/protein-biology-application-notes/simultaneous-dual-emission-detection-luciferase-reporter-assays.html. Accessed 28 Nov 2022.
28. Gomi K, Kajiyama N. Oxyluciferin, a luminescence product of firefly luciferase, is enzymatically regenerated into luciferin. J Biol Chem. 2001;276:36508–13.
29. Cutrona MB, Simpson JC. A high-throughput automated confocal microscopy platform for quantitative phenotyping of nanoparticle uptake and transport in spheroids. Small. 2019;15:1902033.
30. Warrick JW, Murphy WL, Beebe DJ. Screening the cellular microenvironment: a role for microfluidics. IEEE Rev Biomed Eng. 2008;1:75–93.
31. Yurdagul A Jr, Finney AC, Woolard MD, Orr AW. The arterial microenvironment: the where and why of atherosclerosis. Biochem J. 2016;473:1281–95.
32. Northcott JM, Dean IS, Mouw JK, Weaver VM. Feeling stress: the mechanics of cancer progression and aggression. Front Cell Dev Biol. 2018;6:17
33. Liu Q, Luo Q, Ju Y, Song G. Role of the mechanical microenvironment in cancer development and progression. Cancer Biol Med. 2020;17:282–92.
34. Mao X, Xu J, Wang W, Liang C, Hua J, Liu J, et al. Crosstalk between cancer-associated fibroblasts and immune cells in the tumor microenvironment: new findings and future perspectives. Mol Cancer. 2021;20:131.
35. Seidman MA, Mitchell RN, Stone JR. Pathophysiology of atherosclerosis. In: Cellular and molecular pathobiology of cardiovascular disease. Willis MS, Homeister JW, Stone JR, editors. Academic Press; 2014. pp. 221–37.
36. Duval K, Grover H, Han LH, Mou Y, Pegoraro AF, Fredberg J, et al. Modeling physiological events in 2D vs 3D cell culture. Physiology (Bethesda). 2017;32:266–77.
37. Park D, Son K, Hwang Y, Ko J, Lee Y, Doh J, et al. High-throughput microfluidic 3D cytotoxicity assay for cancer immunotherapy (CACI-IMPACT platform). Front Immunol. 2019;10:1133.
38. Yu J, Lee S, Song J, Lee SR, Kim S, Choi H, et al. Perfusable micro-vascularized 3D tissue array for high-throughput vascular phenotypic screening. Nano Converg. 2022;9:16.
39. Chi CW, Lao YH, Rezwanuddin AHR, Benoy EC, Li C, Dereli-Korkut Z, et al. High-throughput tumor-on-a-chip platform to study tumor-stroma interactions and drug pharmacokinetics. Adv Healthc Mater. 2020;9e2000880.
40. Haraguchi Y, Shimizu T, Sasagawa T, Sekine H, Sakaguchi K, Kikuchi T, et al. Fabrication of functional three-dimensional tissues by stacking cell sheets in vitro Nat Protoc. 2012;7:850–8.
41. Mosaad EO, Chambers KF, Futrega K, Clements JA, Doran MR. The microwell-mesh: a high-throughput 3D prostate cancer spheroid and drug-testing platform. Sci Rep. 2018;8:253.
42. Salerno A, Cesarelli G, Pedram P, Netti PA. Modular strategies to build cell-free and cell-laden scaffolds towards bioengineered tissues and organs. J Clin Med. 2019;8:1816.
43. Chiu LLY, Chu Z, Radisic M. Tissue engineering. In: Comprehensive nanoscience and technology. Andrews DL, Scholes GD, Wiederrecht GP, editors. Academic Press; 2011. pp. 175–211.
44. Xin X, Wu Y, Zhang R, Yang ST. A fluorescent 3D cell culture assay for high throughput screening of cancer drugs down-regulating survivin. J Biotechnol. 2019;289:80–7.
45. Martin HL, Adams M, Higgins J, Bond J, Morrison EE, Bell SM, et al. High-content, high-throughput screening for the identification of cytotoxic compounds based on cell morphology and cell proliferation markers. PLoS One. 2014;9:e88338.
46. Jaiswal PK, Goel A, Mittal RD. Survivin: a molecular biomarker in cancer. Indian J Med Res. 2015;141:389–97.
47. Zhang YS, Khademhosseini A. Advances in engineering hydrogels. Science. 2017;356:eaaf3627.

48. Sudhakar CK, Upadhyay N, Jain A, Verma A, Charyulu RN, Jain S. Hydrogels—promising candidates for tissue engineering. In: Nanotechnology applications for tissue engineering. Thomas S, Grohens Y, Ninan N, editors. William Andrew Publishing; 2015. pp. 77–94.
49. Lee SY, Hwang HJ, Ku B, Lee DW. Cell proliferation receptor-enhanced 3d high-throughput screening model for optimized drug efficacy evaluation in breast cancer cells. Anal Chem. 2022;94:11838–47.
50. Ma X, Dewan S, Liu J, Tang M, Miller KL, Yu C, et al. 3D printed micro-scale force gauge arrays to improve human cardiac tissue maturation and enable high throughput drug testing. Acta Biomater. 2019;95:319–27.
51. Lee J, Shin D, Roh JL. Development of an in vitro cell-sheet cancer model for chemotherapeutic screening. Theranostics. 2018;8:3964–73.
52. Han SB, Shin YJ, Hyon JY, Wee WR. Cytotoxicity of voriconazole on cultured human corneal endothelial cells. Antimicrob Agents Chemother. 2011;55:4519–23.
53. Chitty JL, Skhinas JN, Filipe EC, Wang S, Cupello CR, Grant RD, et al. The mini-organo: a rapid high-throughput 3d coculture organotypic assay for oncology screening and drug development. Cancer Rep (Hoboken). 2020;20:131.
54. Takezawa T, Mori Y, Yoshizato K. Cell culture on a thermo-responsive polymer surface. Biotechnology (N Y). 1990;8:854–6.
55. Metzger W, Sossong D, Bächle A, Pütz N, Wennemuth G, Pohlemann T, et al. The liquid overlay technique is the key to formation of co-culture spheroids consisting of primary osteoblasts, fibroblasts and endothelial cells. Cytotherapy. 2011;13:1000–12.
56. Nguyen LTH, Muktabar A, Tang J, Wong YS, Thaxton CS, Venkatraman SS, et al. The Potential of fluocinolone acetonide to mitigate inflammation and lipid accumulation in 2D and 3D foam cell cultures. Biomed Res Int. 2018. https://doi.org/10.1155/2018/3739251.eCollection.
57. Rakshit M, Darwitan A, Muktabar A, Das P, Nguyen LTH, Cao Y, et al. Anti-inflammatory potential of simvastatin loaded nanoliposomes in 2D and 3D foam cell models. Nanomedicine. 2021;37:102434.
58. Puls TJ, Tan X, Husain M, Whittington CF, Fishel ML, Harbin SLV. Development of a novel 3D tumor-tissue invasion model for high-throughput, high-content phenotypic drug screening. Sci Rep. 2018;8:13039.
59. Dykens JA, Will Y. Mitochondrial toxicity. In: Encyclopedia of toxicology (3rd edition), Wexler P, editor. Academic Press; 2014. pp. 349–53.
60. Invitrogen. Click Chemistry—Section 3.1. In: The molecular probes handbook. Thermofisher scientific. https://www.thermofisher.com/us/en/home/references/molecular-probes-the-handbook/reagents-for-modifying-groups-other-than-thiols-or-amines/click-chemistry.html. Accessed 28 Nov 2022.
61. Hamelik RM, Krishan A. Click-iT^{TM} assay with improved DNA distribution histograms. Cytom A. 2009. https://doi.org/10.1002/cyto.a.20780.
62. Leung CM, de Haan P, Bouchard KR, Kim G-A, Ko J, Rho HS, et al. A guide to the organ-on-a-chip. Nat Rev Methods Primers. 2022. https://doi.org/10.1038/s43586-022-00118-6.
63. Biotium. NucView Caspase-3 Substrates. https://biotium.com/technology/nucview-caspase-3-substrates/?keyword=%2Bcaspase%20inhibitors&creative=&msclkid=e7c42cf52a311c0c73b74f713737fd4d&utm_source=bing&utm_medium=cpc&utm_campaign=NucView&utm_term=%2Bcaspase%20inhibitors&utm_content=NucView. Accessed 28 Nov 2022.
64. Parrish J, Lim KS, Baer K, Hooper GJ, Woodfield TBF. A 96-well microplate bioreactor platform supporting individual dual perfusion and high-throughput assessment of simple or biofabricated 3D tissue models. Lab Chip. 2018;18:2757–75.
65. Hu X, Zhao S, Luo Z, Wang F, Zhu J, Chen L, et al. On-chip hydrogel arrays individually encapsulating acoustic formed multicellular aggregates for high throughput drug testing. Lab Chip. 2020;20:2228–36.
66. Hwang HH, You S, Ma X, Kwe L, Victorine G, Lawrence N, et al. High throughput direct 3D bioprinting in multiwell plates. Biofabrication. 2021. https://doi.org/10.1088/1758-5090/ab89c.
67. Yang C, Luo J, Polunas M, Bosnjak N, Chueng SD, Chadwick M, et al. 4D-printed transformable tube array for high-throughput 3d cell culture and histology. Adv Mater. 2020;32:e2004285.

Publisher's Note Springer Nature remains neutral with regard to jurisdictional claims in published maps and institutional affiliations.

Springer Nature or its licensor (e.g. a society or other partner) holds exclusive rights to this article under a publishing agreement with the author(s) or other rightsholder(s); author self-archiving of the accepted manuscript version of this article is solely governed by the terms of such publishing agreement and applicable law.